151406

İSTANBUL TECHNICAL UNIVERSITY ★ INSTITUTE OF SCIENCE AND TECHNOLOGY

ANALYSIS OF FLUID MECHANIC PROBLEMS USING A FINITE ELEMENT METHOD

Ms.c. Thesis

Ayşe Gül GÜNGÖR

(511001201)

Date of submission : April 26, 2004

Date of defence examination : May 20, 2004

Supervisor (Chairman) : Assoc. Prof. Dr. F. Oğuz EDİS

Members of the Examining Committee : Prof.Dr. A. Rüstem ASLAN

Prof.Dr. Adil YÜKSELEN

MAY 2004

151406

İSTANBUL TEKNİK ÜNİVERSİTESİ ★ FEN BİLİMLERİ ENSTİTÜSÜ

AKIŞKANLAR MEKANİĞİ PROBLEMLERİNİN SONLU ELEMANLAR YÖNTEMİ İLE İNCELENMESİ

YÜKSEK LİSANS TEZİ

Ayşe Gül GÜNGÖR

(511001201)

Tezin Enstitüye Verildiği Tarih : 26 Nisan 2004

Tezin Savunuldugu Tarih : 20 Mayıs 2004

Tez Danişmani : Doç. Dr. F. Oğuz EDİS

Diger Juri Üyeleri : Prof.Dr. A. Rüstem ASLAN

Prof.Dr. Adil YÜKSELEN

MAYIS 2004

ACKNOWLEDGMENTS

I would like to thank my advisor Assoc. Prof. Dr. F. Oğuz Edis for his unrestricted support during this study. This study would never be possible without his encouragement and assistance. I also thank to my advisor Dr. Suresh Menon, Professor of Aerospace Engineering at GATECH, for giving permission to come to Turkey and finish this study. I would also like to thank to my friend Cavit Çınar for his contributions to this study.

I also would like to thank to my family for their support and encouragement at every step of my life.

Ayşe Gül GÜNGÖR

May, 2004

TABLE OF CONTENTS

LIST OF TABLES

LIST OF FIGURES

LIST OF SYMBOLS

F_i	: Body force
N_i	: Basis functions
Re	: Reynolds number
p	: Pressure
ρ	: Density
t	: Time coordinate in physical plane
τ	: Time coordinate in transformed plane
u	: Velocity vector
u^*	: Intermediate velocity vector
x, y, z	: Cartesian coordinates in physical plane
Γ	: Integration domain boundary
Ω	: Integration domain
Δt	: Time step
ϕ	: Auxiliary potential function
μ	: Viscosity
μ_b	: Bulk viscosity
ω	: Angular velocity or vorticity
τ_{ij}	: Shear stress
q_j	: Heat flux
W	: Weighting function
e	: Internal energy
h	: Enthalpy
α	: Upwinding coefficient
Δx	: Element length in the cartesian coordinate
δ_{ij}	: Kronecker delta function

AKIŞKANLAR MEKANİĞİ PROBLEMLERİNİN SONLU ELEMANLAR YÖNTEMİ İLE İNCELENMESİ

ÖZET

Daimi olmayan akış problemlerini, birçok mühendislik problemleri ile çözme isteği geometrik olarak kompleks problemlere uygun algoritmaların geliştirilmesine neden olmaktadır. Bu tip problemleri çözmek için kullanılan yöntemler dört ana başlık altında sınıflandırılabilir: Sonlu Farklar Yöntemi, Sonlu Hacimler Yöntemi, Sonlu Elemanlar Yöntemi ve Sınır Eleman Yöntemi. Bu çalışmada bu tip problemleri çözmek için Sonlu Elemanlar yöntemi kullanılacaktır. Sonlu Elemanlar yöntemi akış alanının sonlu küçük elemanlar ile modellenmesi prensibine dayanır.

Üç boyutlu cisimler etrafındaki akışın modellenmesi hesaplamalı akışkanlar mekaniğinin temel çıkış noktalarındandır. Geometrinin ve akış alanının kompleks olması üç boyutlu hesaplamayı güçleştirir. Akış alanı farklı tipte elemanlar ile modellenebilir. Üç Boyutta kullanılan elemanlar, tetrahedral, hexahedral, prizmatik elemanlardır. Akış alanının uygun elemanlar ile modellenmesi çözümün doğruluğunu ve hassasiyetini artırır. Üç boyutlu ağların oluşturulmasında tetrahedral elemanlar hexahedral elemanlara göre kompleks geometrilerin modellenmesi açısından esneklik sağlar. Buna rağmen sınır tabakanın tetrahedral elemanlar ile modellenmesi daha zordur. Bu alanlarda çözüm gradyenleri yüzeye dik doğrultuda oluşur, buda bu bölgelerde yüksek açıklık oranlı elemanlar kullanma gerekliliğini ortaya koyar. Yapısal gridler viskoz bölgelerdeki akışların modellenmesinde etkilidirler. Üç boyutta kullanılan diğer bir eleman tipi de prizmatik elemanlardır. Bu tip ağlar cismin yüzeyini saran üçgen yüzeylerden ve yüzeye dik doğrultuda dörtgen yüzeylerden oluşur. Prizmatik ağlar akışa dik doğrultuda çok yüksek açıklık oranına, akış doğrultusunda geometrik esnekliğe sahiptirler.

Üç boyutlu viskoz akış problemlerinin modellenmesinde prizmatik elemanların kullanılması literatürde gelişmekte olan bir konudur. Bu çalışmada, sınır tabaka bölgesinin prizmatik elemanlar geri kalan çözüm bölgesinin tetrahedral elemanlar ile modellendiği, üç boyutlu sıkıştırılamaz, viskoz akış problemlerinin çözümünde kullanılacak bir sonlu elemanlar uyarlamasi gerçekleştirilmiştir.

ANALYSIS OF FLUID MECHANIC PROBLEMS WITH FINITE ELEMENT METHOD

SUMMARY

Finite element method for fluid flow problems are represented in this study. The governing equations are written in non dimensional form and the Fractional Step method is employed to time discretization. Galerkin Finite Element method is used for the finite element discretization of space for the unsteady incompressible Navier Stokes equations.

The Pseudo-second order velocity/first order pressure interpolation elements are used in this study. These elements satisfy the div-stability condition and using these elements is expected to reduce the memory requirement.

The hybrid tetra elements are analyzed in this study. Hybrid tetra grids consist of layers of prism elements near the boundary surfaces and tetrahedral elements in the interior region. As compared with the pure tetrahedral grids, hybrid grids allow more adequate modeling of the close-to-wall physics of the flow. Prism elements are split into tetrahedral elements for the solutions.

The purpose of this study is to analyze the fluid flow problems with finite element method using pseudo-second order velocity/first order pressure interpolation elements and hybrid tetra grids.

Three dimensional lid driven cavity flow is analyzed. Results are obtained for using the pseudo-second-order velocity interpolation elements for tetra and hybrid tetra grids. Comparison with other numerical data is presented.

A three dimensional analysis of human nasal cavity is also studied. The objective of this study is to examine the relationships between nasal geometry and flow. A three dimensional computational model of airflow in the human nasal cavity is presented to gain more information about the complex flow pattern in the nose. The model represents the general structure of the nose with some geometric simplifications. The use of a finite element numerical approach with hybrid tetra grids with pseudo-second order velocity elements will provide detailed information of the velocity field in every location in the nasal cavity.

1. INTRODUCTION

The equations governing the fluid flow problem are the continuity (conservation of mass), the Navier Stokes (conservation of momentum), and the energy equation. These equations are coupled non-linear partial differential equations. For incompressible, viscous flows these equations can be reduced to a simple form. If these equations can be made linear, or the nonlinear terms are small compared to other terms (e.g. creeping flow) so they can be neglected and the solution can easily found with analytical methods. However, for most flows these terms can not be neglected, and then numerical methods are needed to obtain solutions.

In Computational Fluid Dynamics approach, these differential equations are replaced with a set of algebraic equations which is also called discretization. These discretization techniques are grouped into four branches: Finite Difference Method, Finite Volume Method, Finite Element Method and Boundary Element Method.

The Finite Difference method and Boundary Element method have widely been used for numerical computations and they are still being used.

Finite Difference methods has been accepted as the most popular computation method in CFD. They are quite simple in formulation and lead to highly accurate resuts. However, restrictions to geometry shapes are of great disadvantage of Finite Difference method.

Finite Element method is the most popular method for flow calculations [1].Easy handling of complex geometries, simple solution algorithms and elegant mathematical theory of the Finite Element method has enabled it to become a competitive method with widely accepted Finite Difference and Finite Volume methods.

The Finite Element is an approximate method of solving differential equations of boundary and/or initial value problems. In Finite Element Method, the infinite degrees freedom of the system is discretisized or replaced by a finite number of known parameters.

The Finite Element Method can be explained in six simple step:

1. Discretization: The problem domain is discritized into a collection of simple shapes, or elements.

2. Element Equations: These equations are developed using the physics of the problem, generally Galerkin's Method or variational principles.

3. Assembly: The element equations for each element in the Finite Element Method mesh are assembled into a set of global equations that model the properties of the entire system.

4. Application of Boundary Conditions: Solutions can not be obtained unless the boundary conditions are applied. Imposing the boundary conditions modifies the global equations.

5. Solution for Unknowns: The modified global equations are solved for the primary unknowns at the nodes.

6. Calculation of Derived Variables: These variables are calculated using the nodal values of the primary variables.

The Finite Element Method has been applied to several scientific and technological problems [1, 2, 3, 4]. It is first used by aircraft structural engineers in order to analyze large aerospace structures. It has become a very common technique for the computer solution of complex problems. At present, the Finite Element Method represents a most general analysis tool and is used practically all fields of engineering analysis, Structural and Solid Mechanics, Heat Transfer or Lubrication problems and nonstructural problems which was initiated by Zienkiewicz.

In this study, the steady incompressible viscous flows are considered. The governing equations are the Navier-Stokes Equations and the Continuity equation..

The time integration of the governing equations is carried out by Fractional Step method (see Reference [5]). This method basically segregates the pressure effects at the first step of the computation. An intermediate velocity is calculated at a given time step and the intermediate velocity is corrected to satisfy the continuity using the pressure at the new time step which is found using the divergence of the intermediate velocity.

The Galerkin Finite Element method is used to discritize the equations for incompressible viscous flow. In the Galerkin method, the approximation functions are used as weighting functions.. The Streamline-Upwind-Petrov Galerkin method is used to stabilize the solution of classical Galerkin method [6].

In the Galerkin method, the solution domain is discretized into finite number of elements. Choice of the interpolation function for the finite element is one of the most important aspects affecting the accuracy and the computational cost of the resulting scheme. Pseudo-second order velocity/first order pressure interpolation elements are used in this study [7]. These elements satisfy the div stability condition and reduce the memory requirement and CPU time due to the fewer elements for the solution of Poisson equation [7].

When discretizing a structure or a flow domain, type of the element that suites the problem best can be decided upon depending on the physical geometry.

For two dimensional problems, 2D elements can be used. These include triangular, rectangular, quadrilateral and parallelogram elements. Triangular elements are the most basic and popular elements for two dimensional flow. However quadrilateral elements can be more accurate.

In three dimensional problems, the most common used element is tetragonal element. Other elements rectangular prism and hexahedrons are also used in three dimensional geometries.

Finite elements with curved sides, which are called higher order elements, have been developed for the discritization of problems with curved geometries. This higher order elements increase the accuracy of the solution obtained compared with linear elements. However, the higher order elements normally require more memory and increase the computation time. Also mesh generation for geometrically complex problems using high order elements encounters some invalid high order meshes.

Sherwin and Peiro [8] used three different ways –optimization of the surface generation, hybrid meshing with primatic elements near the domain boundaries, and curvature driven surface mesh adaptation - to reduce the problem of invalid high order meshes in their study.

These elements are used to discretize the domain in finite element analysis. Grid generation is an important part in this analysis. If the grid is too coarse, then the element will not give the correct solution. If the grid is too fine, then the computational cost will increase. A fine grid is required when there are high parameter gradients.

Simulation of flows around geometrically complex bodies is a major issue in computational fluid mechanics. Generation of a body-conforming grid proves to be a difficult task. Tetrahedral grids provide flexibility in three dimensional geometries since they can cover complicated geometries more easily compared to hexahedral grids. However, for regions where the main solution gradients occur in the direction normal to the surface requires very large aspect ratio elements. In these regions it is very difficult to generate tetrahedral elements. An alternative is to use prismatic grids. Such grids consist of triangular faces that cover the body surfaces, while quadrilateral faces extend in the direction normal to the surface [9]. Another studies are based on the refinements of the grid locally to resolve detected flow features [10]. A special type of adaptive refinement of prisms in order to preserve the structure of the mesh along the normal-to-surface direction is explained in detail in the study of Kallinderis [11].

In this study tetrahedral and hybrid tetrahedral grids are used. Hybrid grids consist of layers of prism elements near the boundary surfaces and tetrahedral elements in the interior region. As compared with the pure tetrahedral grids, hybrid grids allow more adequate modeling of the close-to-wall physics of the flow. Boundary layer region are modeled with prismatic elements then these elements split into tetrahedral elements for the solution.

A most common benchmark case 3-D lid driven cavity flow is studied for two different grid structures. Grids used for the simulations and the results are represented in Chapter 6. The results show excellent agreement with the reference data [12].

A simulation of human nasal cavity with Finite Element Method is also represented in this study. Several numerical and experimental studies have been done to analyze the flow in nasal cavity.

Airflow profiles in human nasal passages have been studied experimentally by a number of researchers [13]. These studies do not provide enough quantitative information about the airflow. The numerical studies using realistic nasal geometries are limited with capabilities of the current computers. The study of the Keyhani et al. is the most detailed of the numerical study of the human nasal cavity [14]. They examined airflow through one side of the nose in a three dimensional model.

A numerical simulation of the flow in the human nasal cavity using an AUSM based method is given by Horschler [15]. Computations are performed for inspiration and expiration at rest with two Reynolds numbers and the results show excellent agreement with the experimental data.

The human nose covers a variety of functions such as moistening, tempering and cleaning of the air [16]. Additionally, the sense of smell and the sense of taste are located in the upper part of the nasal cavity. All these functions are strongly influenced by the internal flow conditions. Therefore a detailed investigation of the flow field is essential to enable successful surgery and knowledge of airflow in the human nose is important for understanding many aspects of the biology and pathology of the respiratory tract. A numerical flow simulation can be a useful part of a computer assisted surgery tool [15].

The purpose of this study is to extend these studies by using computational fluid dynamics simulations and to predict the nasal airflow field more accurately. The finite element method is used for this purpose.

The geometry of the calculation domain is defined using a computational tomografic scans of a human healthy adult male. Inspiratory and expiratory cycles are analyzed seperately. The flow is assumed to be laminar and incompressible. For the inhalation phase, a velocity normal to the inlet section is imposed. For the exhalation phase a negative velocity is imposed. A pressure condition is imposed at the outlet. The no-slip boundary condition treats the wall of the nasal airway as a smooth, non-wavy solid wall.

The result presented in Chapter 6 correspond to a velocity of 0.25 m/s at the inlet or a flowrate of 125 ml/s. The calculations and the post processing of the results are carried out on a P4 Pc. The calculation time is close to 72 hours. The grid totally involves 146516 finite elements for pressure and 1172128 for velocity.

The results show similar behavior with experimental and other numerical studies. The corrcet distribution of the pressure is achieved. The velocity has a maximum in the middle part of the nasal cavity.

Governing equations are given in Chapter 2. The finite element discetizations of the governing equations are explained in detail in Chapter 3. Grids used in this study and the division of prismatic elements are given in Chapter 4. Numerical simulation of the human nasal cavity is introduced in Chapter 5, and the results obtained for the three dimensional lid-driven cavity flow and the human nasal cavity flow are reported in Chapter 6. And a brief conclusion is given in Chapter 7.

2. GOVERNING EQUATIONS

The governing equations that describe the flow of fluids are a set of nonlinear partial differential equations, known as the Navier-Stokes equations. These equations are derived by considering the mass, momentum and energy balances for infinitesimal control volume.

The time dependent continuity equation for conservation of mass:

$$\frac{\partial \rho}{\partial x_i}+\frac{\partial}{\partial x_j}\left(\rho u_j\right)=0 \tag{2.1}$$

Time dependent conservation of momentum equations,

$$\frac{\partial}{\partial t}\left(\rho u_i\right)+\frac{\partial}{\partial x_j}\left(\rho u_i u_j\right)=-\frac{\partial p}{\partial x_i}+\frac{\partial \tau_{ij}}{\partial x_j}+\rho \mathrm{F_i} \tag{2.2}$$

And the time dependent conservation of energy equation is given as following

$$\frac{\partial}{\partial t}\left(\rho\left[e+\frac{1}{2}u^2\right]\right)+\frac{\partial}{\partial x_j}\left(\rho u_j\left[h+\frac{1}{2}u^2\right]\right)=\frac{\partial}{\partial x_j}\left(\tau_{\mathrm{jk}}u_k-q_j\right)+\rho \mathrm{F_j u_j} \tag{2.3}$$

The tensor notation is used to simplify the equations. Spatial coordinates x, y, z and the time t are the independent variables. The pressure p, density ρ, temperature T (which is contained in the energy equation) and the velocity vector components, u in the x direction, v in the y direction and w in the z direction are the dependent variables in these equations. Body forces F are also included in these equations.

The shear stress tensor τ_{ij} in the momentum and energy equation can be written according to the Stokes' hypothesis

$$\tau_{ij}=\mu\left(\frac{\partial u_i}{\partial x_j}+\frac{\partial u_j}{\partial x_i}-\frac{2}{3}\frac{\partial u_k}{\partial x_k}\delta_{ij}\right)+\mu_b\frac{\partial u_k}{\partial x_k}\delta_{ij} \tag{2.4}$$

μ is the shear viscosity for deformation and μ_b is the bulk viscosity of the fluid which responsible for energy dissipation in a fluid of uniform temperature during a change in volume at a finite rate [17]. And, Kronecker delta $\delta_{ij} = 0$ for $i \neq j$ and $\delta_{ij} = 1$ for $i = j$.

According to Fourier's law, the heat flux q_j in the energy equation is proportional to the temperature.

$$q_j = -k_c \frac{\partial T}{\partial x_j} \tag{2.5}$$

k_c is the thermal conductivity, e and h represents the internal energy and enthalpy respectively in the energy equation.

These equations can be simplified further for the incompressible fluids (ρ = constant) and under the assumption that the temperature variations are small then viscosity μ may also be taken constant. The energy equation becomes useless for incompressible fluids.

The simplified equations with neglecting the body forces are given as follows:

$$\frac{\partial u_i}{\partial x_i} = 0 \tag{2.6}$$

$$\rho\left(\frac{\partial u_i}{\partial t} + u_j \frac{\partial u_i}{\partial x_j}\right) = -\frac{\partial p}{\partial x_i} + \mu \frac{\partial^2 u_i}{\partial x_j \partial x_j} \tag{2.7}$$

These equations are dimensional. The non-dimensional form of these equations are used in computational studies. These can be made dimensionless by referring all velocities to the free stream velocity V_0 and by referring all dimensions to a characteristic length L. The pressure is made dimensionless with $\rho_0 V_0^2$ and the time is referred to L / V_0. The non dimensional variables are denoted by an asterisk.

$$x_i^* = \frac{x_i}{L}, \qquad p^* = \frac{p - p_0}{\rho_0 V_0^2}, \qquad u_i^* = \frac{u_i}{V_0}, \qquad t^* = \frac{tV_0}{L} \tag{2.8}$$

By substituting these new variables, the non dimensional form of the equations are written as follows;

$$\frac{\partial u_i^*}{\partial x_i^*} = 0 \tag{2.9}$$

$$\frac{\partial u_i^*}{\partial t^*} + u_j^* \frac{\partial u_i^*}{\partial x_j^*} = -\frac{1}{\rho}\frac{\partial p^*}{\partial x_i^*} + \frac{1}{\mathrm{Re}}\frac{\partial^2 u_i^*}{\partial x_j^* \partial x_j^*} \tag{2.10}$$

Here, the non-dimensional parameter is the Reynolds number based on the characteristic length and L and the velocity defined as

$$\mathrm{Re} = \frac{\rho V_0 L}{\mu} \tag{2.11}$$

Reynolds number can be defined as the ratio of the inertial forces to the viscous forces. This dimensionless parameter plays an important role defining the flow characteristics.

For high Reynolds numbers, the viscous effects are confined to a small layer close to the wall for wall bounded flows. This small region is known as the boundary layer where the viscous forces are the same order of the inertia forces.

For very slow motions with large viscosity (low Re number) the viscous forces are considerably greater than the inertia forces and the inertia terms (convective terms in the momentum equation) with respect to the viscous terms can be neglected. This kind of flows are sometimes called creeping motions.

For high Reynolds numbers the flow becomes turbulent.

3. TIME AND SPACE DISCRETIZATION

The temporal and spatial discretizations of the Navier-Stokes equations are presented in this chapter.

3.1 Time Discretization

The time integration of the Navier-Stokes equations is often carried out by means of the fractional step procedure which is first suggested by Chorin (see reference [5]). With Chorin's method at each time step an incomplete form of the momentum equations is integrated to give an approximate velocity field which does not satisfy the continuity, then a correction is applied to that velocity field in order to produce a divergence free velocity field. The correction to the velocity field is called projection step. The basic projection method drops the pressure gradients from the momentum equations. This method requires the use of special boundary conditions for the intermediate velocity field to ensure second order in time behavior.

An alternative to the basic projection method is the pressure correction method. In this method the pressure gradient term retained in the momentum equation, and the Poisson equation is then solved for a pressure correction which is used to correct the intermediate velocity field and satisfy the continuity.

The Fractional step method proposed by Mizukami is used in this study and explained briefly in the next section [18]. This method introduces auxiliary potential function to correct fractional step velocities to obtain divergence free full step velocities [7].

3.1.1 Fractional-Step Method

The fractional-step method is used for the temporal discretization of the Navier-Stokes equations. This method basically segregates the pressure effects at the first step of the computation.

An intermediate velocity field (u_i^*) is calculated from known values at a given time step (n)

$$u_i^* = u_i^n + \Delta t \left\{ \frac{1}{\mathrm{Re}} \frac{\partial^2 u_i^n}{\partial x_j \partial x_j} - u_j^n \frac{\partial u_i^n}{\partial x_j} \right\} \tag{3.1}$$

The pressure for the next time step ($n+1$) is solved using the divergence of this intermediate velocity.

$$\frac{\partial^2 p^{n+1}}{\partial x_j \partial x_j} = \frac{1}{\Delta t} \frac{\partial u_j^*}{\partial x_j} \tag{3.2}$$

The intermediate velocity field is then corrected in the third step to satisfy the continuity, using the pressure at the new time step.

$$u_i^{n+1} - u_i^* = -\Delta t \frac{\partial p^{n+1}}{\partial x_i} \tag{3.3}$$

For the first iteration at each time step p^{n+1} is set to equal p^n. Many implementations of this method can be found in elsewhere [7].

3.1.2 The Time–Step Size

The stability of the computations depends on the time-step size for explicit time stepping schemes. In [19], stability condition for the time-step size of convection – diffusion problem is given as

$$\Delta t \leq \frac{1}{\frac{2}{\mathrm{Re}} \left(\frac{1}{\Delta x_i \Delta x_i} \right) + \frac{|u_i|}{\Delta x_i}} \tag{3.4}$$

where Δx_i denotes element length in the Cartesian coordinate direction x_i.

3.2 Space Discretization

The equations for incompressible viscous flows are discretized in space using Galerkin Finite Element method. Next section describes the use of the Galerkin Finite element method for incompressible viscous flow computations.

3.2.1 Galerkin Finite Element Method

The incompressible Navier Stokes equations are spatially discretized by finite elements. Most finite element methods are based on the Galerkin formulation. The Galerkin finite element method requires that the weight and shape functions must be the same.

The temporally discretized equations in the first section are spatially discretized by Galerkin Method. The weighted residual integrals for equations (3.1) (3.2) and (3.3) are given above respectively

$$\int_{\Omega_e^v} W u_i^* d\Omega_e = \int_{\Omega_e^v} W u_i^n d\Omega_e + \Delta t \int_{\Omega_e^v} W \left[\frac{1}{\mathrm{Re}} \frac{\partial^2 u_i^n}{\partial x_j \partial x_j} - u_j^n \frac{\partial u_i^n}{\partial x_j} \right] d\Omega_e \tag{3.5}$$

$$\int_{\Omega_e^p} W \frac{\partial^2 p^{n+1}}{\partial x_j \partial x_j} d\Omega_e = \frac{1}{\Delta t} \int_{\Omega_e^p} W \frac{\partial u_j^*}{\partial x_j} d\Omega_e \tag{3.6}$$

$$\int_{\Omega_e^v} W u_i^{n+1} d\Omega_e = \int_{\Omega_e^v} W u_i^* d\Omega_e - \Delta t \int_{\Omega_e^v} W \frac{\partial p^{n+1}}{\partial x_j} d\Omega_e \tag{3.7}$$

The solution domain is discretized into a finite number of elements Ω_e. Different types of elements are used for pressure and velocity. This will be explained in the next section. W is the weighting function, Ω_e^v is the velocity element and Ω_e^p is the pressure element. In equations (3.5) and (3.7), fractional-step and full-step velocity components are unknown. In equation (3.6), the pressure is unknown. These unknowns will be approximated by shape functions [7].

After choosing appropriate shape functions for velocity and pressure, Galerkin integral matrix equations can be cast.

For the Galerkin formulation, the weight functions are selected identical to the unknown field shape functions. The classical Galerkin formulation is optimal for the discretization of elliptic equations. However the equations governing viscoelastic flows, or heat transportation are hyperbolic. For this kind of equations, the classical Galerkin formulations will lead to spurious oscillations in the results. Therefore, modified weight functions are used to improve solutions.

In this study, stabilizations of this kind of oscillations are based on the Streamline-Upwind Petrov-Galerkin (SUPG) method. The SUPG method is currently one of the most popular methods for advection-diffusion problems due to its inherent consistency and efficiency in avoiding the spurious oscillations obtained from the classical Galerkin method when there are discontinuities in the solution.

For this purpose second order term is added for upwinding. The general steps and the application of this term are given in ref. 7.

With the addition of the upwinding term into the momentum equation and using the appropriate weighting functions, the general form of Galerkin integral equations are given [7] in the following form,

$$\begin{aligned}\int_{\Omega_e^v} N_q u_i^* d\Omega_e &= \int_{\Omega_e^v} N_q u_i^n d\Omega_e \\ &- \Delta t \int_{\Omega_e^v} \left[N_q u_j^n \frac{\partial u_i^n}{\partial x_j} + \frac{1}{\mathrm{Re}} \frac{\partial N_q}{\partial x_j} \frac{\partial u_i^n}{\partial x_j} + \alpha u_j^n \frac{\partial N_q}{\partial x_j} u_k^n \frac{\partial u_i^n}{\partial x_k} \right] d\Omega_e \\ &+ \Delta t \int_{\Gamma_e^v} N_q \left(\frac{1}{\mathrm{Re}} \frac{\partial u_i^n}{\partial x_j} + \alpha u_j^n u_k^n \frac{\partial u_i^n}{\partial x_k} \right) n_j d\Gamma_e\end{aligned} \tag{3.8}$$

$$\int_{\Omega_e^p} \frac{\partial P_l}{\partial x_j} \frac{\partial p^{n+1}}{\partial x_j} d\Omega_e = -\frac{1}{\Delta t} \int_{\Omega_e^p} P_l \frac{\partial u_j^*}{\partial x_j} d\Omega_e + \int_{\Gamma_e^p} P_l \frac{\partial p^{n+1}}{\partial x_j} n_j d\Gamma_e \tag{3.9}$$

$$\int_{\Omega_e^v} N_l u_i^{n+1} d\Omega_e = \int_{\Omega_e^v} N_l u_i^{*} d\Omega_e - \Delta t \int_{\Omega_e^v} N_l \frac{\partial p^{n+1}}{\partial x_j} d\Omega_e \tag{3.10}$$

where N_l and P_l are the shape functions for velocity and pressure elements respectively. Γ_e^v and Γ_e^p are the boundaries and n_j is the unit normal of this boundaries. In the upwinding term, α is related to the velocity components and the element lengths in local coordinates.

3.2.2 Pseudo-Quadratic Velocity Interpolation Elements (pP2P1)

In the Galerkin formulation the solution domain is discretized into a finite number of elements. Using linear functions, the elements will be line segments for one-dimensional problems, triangles or quadrilaterals for two-dimensional problems, and tetrahedral, prisms or hexahedrals for three-dimensional problems. The approximation functions are defined on these elements. The order of the approximation function is related to the order of the derivatives in the weighted residual statement.

The amount of data to be stored and processed per element increases with increasing degree of the approximation functions. In order to perform computationally effective simulations, it is important to use approximation functions of lowest possible degree.

Choice of the interpolation function for the finite element is one of the most important aspects affecting the accuracy and computational cost of the resulting schema. Pseudo-quadratic velocity interpolation elements (pP2P1) are used in this study [7].

Pseudo-second order velocity/first order pressure interpolation elements are constructed by dividing the pressure element into sub elements.

Pseudo-quadratic velocity interpolation on a triangular element (pP2P1) is achieved by inserting mid-side nodes to the pressure element and interconnecting these to give four sub-elements over which the velocity is interpolated linearly. Three dimensional elements are formed similarly which gives eight sub-elements. Figure 3.1 shows these elements and node numbering.

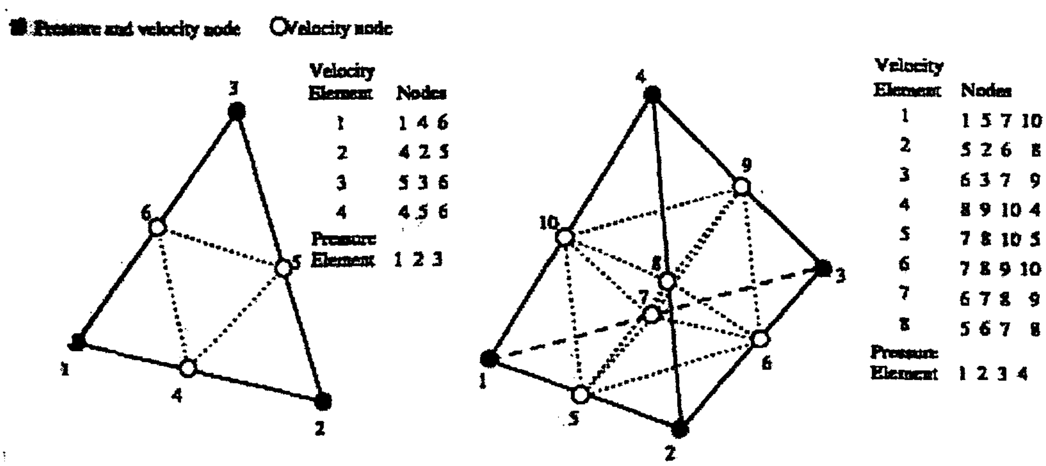

Figure 3.1. Linear velocity / pseudo-quadratic pressure interpolation elements in 2-D and 3-D [7].

At nodes 1,2,3 of the triangle and nodes 1,2,3,4 of the tetrahedra, both the velocity components and the pressure is calculated. At remaining nodes, the velocity is calculated only.

These element pairs satisfy the div-stability condition which is also known as the 'Ladyzhenskaya-Babuska-Brezzi'(LBB) condition. This condition ensures that no oscillations occur in the pressure field. Also, using these elements, when compared to an equivalent first-order pair formulation, is expected to reduce the memory requirement and the CPU time due to the fewer elements used in the solution of the Poisson equation for pressure [7].

4. NUMERICAL ASPECTS

In numerical studies, the process of grid generation is used to decompose the computational domains into finite elements or finite volumes. The efficiency of the analysis frequently related to an effective finite mesh.

In this study tetrahedral grids and hybrid tetrahedral grids consisting of layers of prism elements near the boundary surfaces and tetrahedral elements in the interior region are used.

In this chapter, the general information about grids used in Finite Element Analysis is presented and division of prism elements to tetrahedral elements is explained.

4.1 Grids Used in Finite Element Analysis

A good or appropriate mesh is one that enables accurate resolution of the underlying physical phenomena, yet is coarse enough to allow a fast solution time. Mesh generation is the process of dividing the analysis domain into a number of discrete parts or finite elements. Flow variables are calculated at finite number of points placed on the elements, on the nodes.

Choosing the correct mesh density required to solve a problem is an important part in the Finite Element Analysis. If the mesh is too coarse, then the element will not allow a correct solution to be obtained. Alternatively, if the mesh is too fine, the cost of analysis in computing time can be out of proportion to the results obtained. A fine mesh is required where there are high parameter gradients and a coarse mesh is sufficient in areas that have result contours of reasonably constant slope. Grid generation is closely related to the solution algorithm and the accuracy of the result strongly depends on the quality of the mesh employed.

Commonly used mesh generation techniques can be classified as structured, block - structured and unstructured. The techniques for obtaining structured grids are based

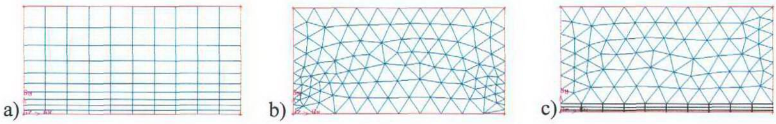

Figure 4.1 An example of grid for flat plate a) Structured b) Unstructured c) Hybrid grid

on rules for the grid-subdividing of geometries and mapping techniques. Structured grids can be generated easily. However for complex geometries it may not be possible to generate structured grids. Unstructured grids have been one of the most popular research areas in grid generation. Unstructured grids are usually generated with triangular or tetrahedral elements in two- and three dimensions respectively. It is an automatic grid generation and easy to apply for complex geometries. On the other hand unstructured grids are poor representation of the boundary layer near the solid body as shown in Figure 4.1b. When using meshing schemes, it is important to be able to generate anisotropic meshes. For thin structures, elements must be used that are thin in one direction and long in the other two. In fluid flows, boundary layers need to be modeled with very thin elements aligned with the boundary. In Figure 4.1, a two dimensional structured, unstructured and hybrid mesh is represented for a flat plate.

For three dimensional geometries, it can be very difficult to generate block-structured grids and even impossible to generate structured grids. An alternative to structured grids is the use of tetrahedral grid. Tetrahedral grids provide flexibility in three dimensional grid generations since they can cover complicated topologies more easily. However, generation of tetrahedral cells for boundary layers is quite difficult. In Figure 4.2., an unstructured tetrahedral mesh for a cubic cavity is shown. It is generated using a commercial mesh generation software for the solution of the cubic cavity flow.

Structured grids are superior in capturing the directionality of the flow field in viscous regions. Studies to overcome this difficulty usually result in techniques to generate structured grids for regions where high aspect ratio elements are required or techniques where elements with different geometries such as quadrilaterals, bricks or prismatic elements are used for directional refinement.

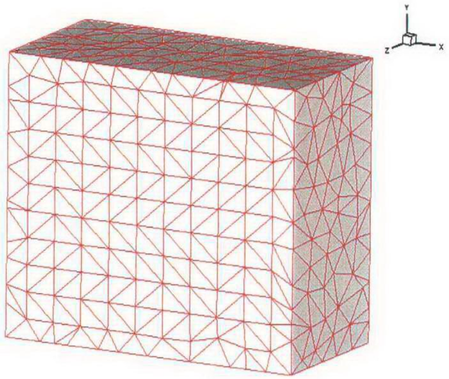

Figure 4.2 An unstructured mesh for a cubic cavity

Prismatic grids consist of triangular faces that cover the body surface, while quadrilateral faces extend in the direction normal to the surface [9]. The prismatic cells can have very high aspect ratio and provides geometrical flexibility in the lateral directions.Additionally, the structured nature of the prismatic grid allows simple implementation of algebric turbulence models and semi-implicit numerical schemes [20].

The areas between different prismatic layers covering the surfaces of the domain can be quite irregular. Prismatic elements cannot cover these domains. Also, the relevant flow features in these regions do not usually exhibit the strong directionality that the viscous regions have. Tetrahedral elements appear to be appropriate for these regions. The triangular faces of the tetrahedrals can match the corresponding triangular faces of the prisms [11]. These kind of grids are known as hybrid grids.

Figure 4.3 shows a hybrid grid for cubic cavity. Prismatic elements are used in boundary layer region where high aspect ratio required and tetrahedral elements are used which covers the rest of the computational domain. In comparison to pure tetrahedral grids, hybrid tetrahedral grids with near-surface prism layers allow for a more adequate modeling of the close-to-wall physics of the flow. The structured nature of the prisms in the normal to surface direction exploits the advantages of

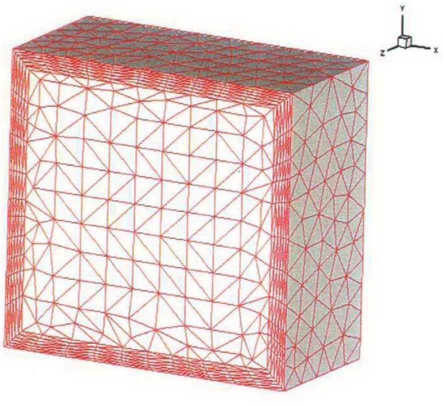

Figure 4.3 A hybrid mesh for cubic cavity

traditional structured grid approaches. The prismatic grid offers good orthogonality and clustering capabilities.

Tetrahedral grids and hybrid tetrahedral grids consisting of layers of prism elements near the boundary surfaces and tetrahedral elements in the interior region are used in this study.

4.2 Division of Prismatic Elements

Since the code that is used for the simulations [7] can solve only for tetrahedral elements, the prismatic elements are split into tetrahedral elements. The division of prismatic elements and the problems that are encountered during this step is explained in detail in this section

A prismatic elemen has two triangular and three quadrilateral faces.The quadrilateral faces and the node numbering of a prismatic element is shown in Figure 4.4.The quadrilateral faces of the prisms are divided into triangles. By dividing these three quadrilateral faces into two triangles, eight different division types can be possible for one prismatic element. All quadrilateral faces are not divided along the direction which is normal to the surface. In this way the structure of the grid along the normal-to-surface direction is preserved.

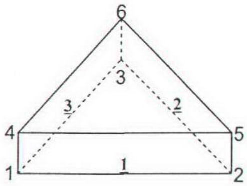

Figure 4.4 Prismatic elements in 3-D

The division type of the quadrilateral faces can be split into two different forms. *A* is a division type which starts from the first node of the quadrilateral face and *B* starts from the second node of the quadrilateral face. The division type of the quadrilateral faces and the node numbering for the trianguls are given in detail in Table 4.1.

By dividing these three qudrilateral faces, eight different division types for a prismatic element can be achieved. However, only six of these eight can create tetrahedral elements.

A division type of a prismatic element and the local node numbering is shown in Figure 4.5 for the division code of *BBB*. One prismatic element creates three tetrahedrals which have the structure of normal-to-surface direction.

In Table 4.2, the division codes of a prismatic element and the node numbering of the tetrahedrals that are formed after the division of qudrilateral faces are given in detail. The division code refers to the first, second and third quadrilateral face's division types of a prismatic element.

Table 4.1. Details of the division types of the quadrilateral faces and the node numbering of the triangular elements.

Face No	Division type	Node numbering of Triangle 1	Node numbering of Triangle 2
1	A	125	154
	B	124	254
2	A	236	265
	B	235	365
3	A	146	163
	B	143	463

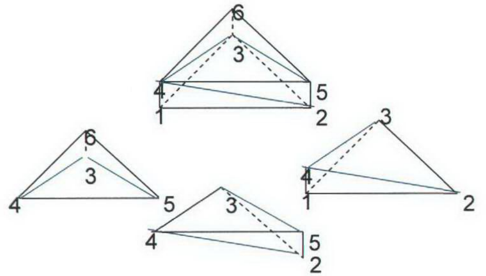

Figure 4.5 A division type of a prismatic element

As shown in Table 4.2, two division types *AAB* and *BBA* can not create tetrahedral elements. In Figure 4.6a the negative division type of an element is shown for the division code of *AAB*. This is the first problem that is encountered while splitting the prismatic element.

Another problem is revealed while dividing all prismatic elements in the computational domain. In the same row, two prismatic elements have one common quadrilateral face. It is obligatory to divide these faces with the same form. Figure 4.6b shows the negative division type in a row.

A simple code is developed in Fortan 77 language to split prismatic elements. The program determines all the neighboring elements and common faces of these elements and divides them with the same form.

Table 4.2. Details of the division codes of a prismatic element and the node numbering of the tetrahedral elements.

Division		Node numbering of	
code	Tetra 1	Tetra 2	Tetra 3
AAA	1256	1546	1326
AAB	---	---	---
ABA	1465	1563	2351
ABB	4563	2351	1435
BAA	1263	2654	1462
BAB	1243	2654	2643
BBA	---	---	---
BBB	4563	1432	2354

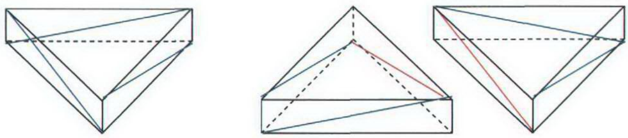

a) b)

Figure 4.6 a) Negative division type of prism b) Negative division type in a row

After dividing all prismatic elements in the computational domain, all elements division types are controlled and searched for any negative division type. As mentioned above a prismatic element can be divided by eight different types but only six of eight creates tetrahedral elements. If any negative type is found, then the program gives a random element number and one of the three quadrilateral faces of this element's division type is change randomly. And this operation continues until all the prismatic elements are divided by the correct division type. After all these steps, all prismatic elements in the computational domain are divided into three tetrahedral elements.

5. MODELLING OF HUMAN NASAL CAVITY

The human nose fulfills a variety of functions such as moistening, tempering and cleaning the air. Additionally, the sense of smell and the sense of taste are located in the upper part of the nasal cavity. All these functions are strongly influenced by the internal flow conditions. Therefore a detailed investigation of the flow field is essential to enable successful surgery. A numerical flow simulation can be a useful part of a computer assisted surgery tool. Several models have been derived to express the relationship between flow rate and resistance [14].

The objective of this study is to examine the relationships between nasal geometry and flow. A three dimensional computational model of airflow in the human nasal cavity is presented to gain more information about the complex flow pattern in the nose. The model represents the general structure of the nose with some geometric simplifications. The use of a finite element numerical approach will provide detailed information of the velocity field in every location in the nasal cavity.

5.1 Modelling

The nasal cavity and turbinates present a complicated three dimensional geometry that limits a detailed analysis of the various geometric and structural parameters that control nasal airflow patterns.

To construct the internal anatomy of the nasal cavity, coronal computed tomography (CT) scans is used. CT scans were 2 mm apart from the nares to choanas along the nasal cavity of a living adult male. In Figure 5.1 every five CT scan is shown, units are given in cm.

These scans then transferred to the computer to create a three dimensional solid model. Only one of the nasal cavities was imaged because the two passages are roughly symmetric and humans generally breathe in a cyclic pattern, alternating between the left and right nasal cavity over a period of a few hours.

Figure 5.1 CT scans of nasal cavity of a healthy adult male.

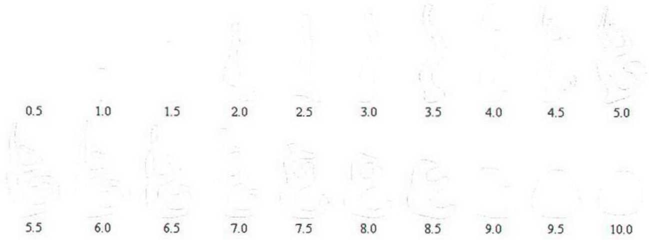

Figure 5.2 Closed curves corresponding to the slices of anatomical data

CAD software is used to create the geometry of the CT scans. A spline command within A-CAD 2000 program is used and the closed curves corresponding to the slices of anatomical data are formed (Figure 5.2).

Three dimensional solid model of the nasal cavity is created by using a commercial software. Solid model of the nasal cavity is shown in Figure 5.3.

Figure 5.3 Solid model of the nasal cavity

6. RESULTS AND DISCUSSION

In the previous chapters, a finite element method for the solution of unsteady, incompressible viscous flows is represented. Prismatic elements and modeling of human nasal cavity are also described.

By using prismatic elements, the body surface is covered with triangles, which provides geometric flexibility, while the structure of the mesh in the direction normal to the surface provides thin prismatic elements suitable for the viscous region.

Three-dimensional lid-driven cavity test problem is analyzed in order to assess the efficiency of the prismatic elements. Result is compared with experimental data.

Computational analysis of nasal airflow patterns is also studied.

Computational meshes for all cases are generated using a commercila grid generation software. The solver modified by Edis [7] is used for the simulations.

6.1 Three-Dimensional Lid-Driven Cavity Flow

Results obtained for laminar, three-dimensional cavity flow is represented in this section. The domain of the flow is a unite cube with the upper boundary ($y = 1$) moved with constant speed in positive x-direction. Other boundaries ($x = 0, x = 1, y = 0, z = 0, z = 1$) are solid walls with no-slip boundary condition. One half of the domain ($0 \leq z \leq 0.5$) is analyzed due to the symmetry of the flow field. The flow domain and the boundary conditions are shown in Figure 6.1. The Reynolds number based on the height of the cavity is 1000. The Drichlet boundary condition for pressure is imposed at the center node of the symmetry plane ($z = 0$) as $p = 0$. The analyses start from zero velocity and pressure initial conditions and continue until the dimensionless time about which the steady state is reached.

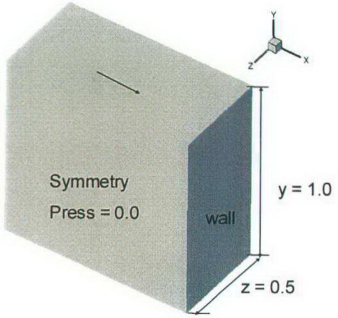

Figure 6.1. Dimensions and boundary conditions for lid driven cavity flow

Two cases are run for this problem. First case is run with tetrahedral elements. Second case is run with hybrid elements (prismatic and tetrahedral elements). In the second case, prismatic elements are divided into tetrahedral elements. One prism is split into three tetrahedral elements. These cases and related information is listed in Table 6.1. Computational meshes for two cases presented in Figure 6.2 and 6.3. A convergence criterion for the pressure solver is 10^{-5}.

Table 6.1. Details of analyses performed for three-dimensional lid-driven cavity flow problem

Case	Element geometry	Element type	Pressure elements	Velocity elements
1	Tetrahedral	pP2P1	7259	58072
2	Prism + Tetrahedral	pP2P1	9331	70416

Three dimensional pressure fields are presented in Figure 6.4 for three dimensional lid-driven cavity flow.

Velocity vector fields on symmetry plane obtained for each analysis is shown in Figure 6.5. The primary vortex caused by the viscous transport of momentum from the lid is apparent in all results. Velocity magnitudes in the flow direction are increasing with increasing distance from the wall at z = 0.

Pressure distributions on the symmetry plane are also shown in Figure 6.5. Tetrahedral grids yields a less oscillatory pressure field.

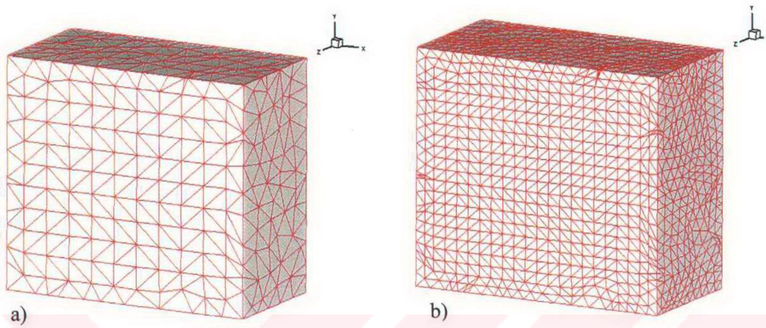

Figure 6.2 Tetrahedral grids for simulations of three dimensional lid-driven cavity flow. a) Pressure grid b) Velocity grid

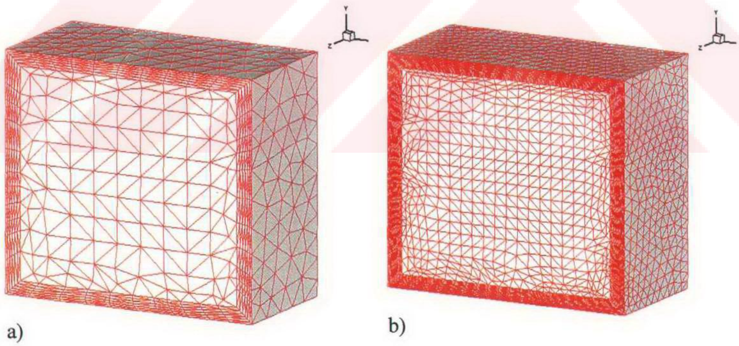

Figure 6.3 Hybrid grids for simulations of three dimensional lid-driven cavity flow.

a) Pressure grid b) Velocity grid

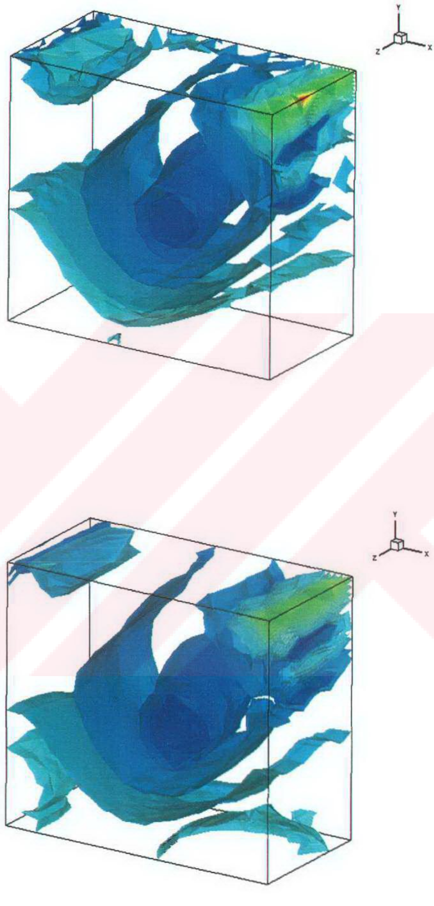

a)

b)

Figure 6.4 Pressure iso-surface plots of lid-driven cavity flow a) tetra grid b) hybrid grid

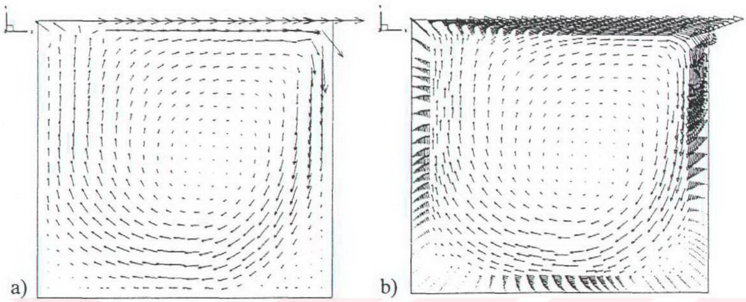

Figure 6.5 Velocity vectors of lid driven cavity flow a) tetra grid b) hybrid grid

Figure 6.6 Pressure contour plots at the symmetry plane of lid driven cavity flow a) tetra grid b) hybrid grid

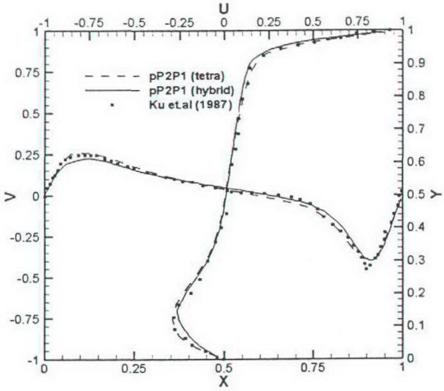

Figure 6.7 Velocity distributions along horizontal and vertical centerlines of the symmetry plane of lid driven cavity flow

Velocity distributions along the horizontal and vertical centerlines of the symmetry plane are shown in Figure 6.7. The results compared with a numerical study [8]. Results for two cases show excellent agreement.

7.2 Human Nasal Cavity Flow

Another study for laminar, three-dimensional human nasal cavity flow is represented in this section. The three dimensional geometric model represents the general structure of the nose with geometrical simplifications.

A uniform flow with 0.25 m/s velocity is imposed as boundary condition throughout the nostril which represents a flow rate of 125 ml/s. For physiological breathing rates, the flow in the nasal cavity is expected to be mainly laminar. Previous experimental and numerical studies indicate that flow is laminar when the half-nasal flow rate is less than 200 ml/s (Hahn et al., 1993, Keyhani et al., 1995). Hence the time dependent of incompressible viscous fluid (air) is analyzed for laminar flow in this study. Reference pressure at nostril end is also given as boundary condition. Other boundaries are solid wall with no-slip boundary condition. The three dimensional model and the boundary conditions are shown in figure 6.8.

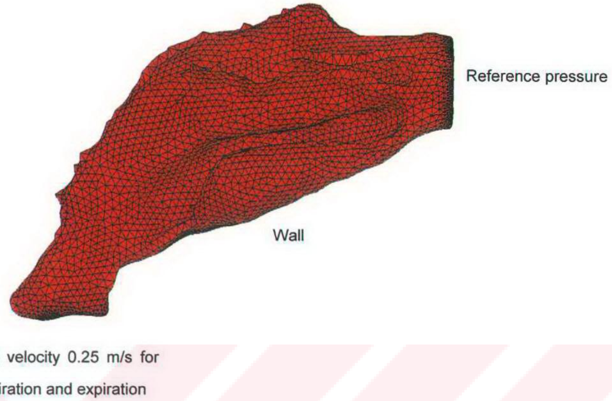

Figure 6.8 Pressure grid for the simulation of the human nasal cavity

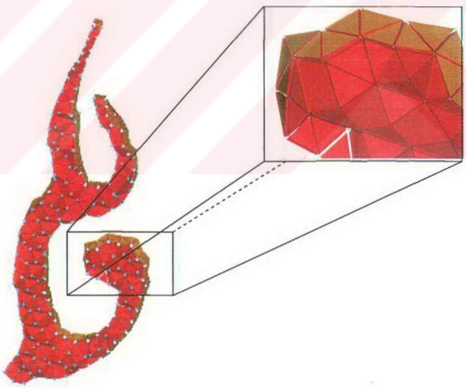

Figure 6.9 Detail view of the pressure grid used for the simulation of the human nasal cavity flow

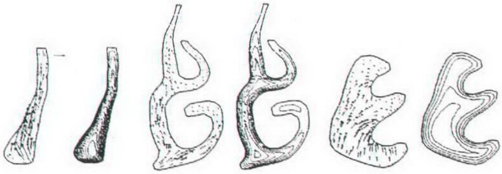

Figure 6.10 Velocity vector plot and velocity magnitude contour maps for inspiratory nasal airflow

Discretization of the solution domain into finite elements is done using a commercial automatic mesh generation software. Hybrid tetrahedral grid is used for the simulation of human nasal cavity flow (Figure 6.8).

Two layers of prismatic elements are constructed to represent the boundary layer affect. Interior region is filled with tetrahedral elements shown in detail in figure 6.9.

The grid generation consists of three steps. First, hybrid grid is generated using a automatic mesh generation software, second prismatic elements are divided into tetrahedral elements and last the pressure elements are subdivided into the velocity elements. The finite element grid used in this study consists of 1,172,128 velocity and 146,516 pressure elements.

A finite element solver (modified by Edis [7], 1998) is used to analyze the flow inside the human nasal cavity.

Inspiratory and expiratory cycles are analyzed separately.Velocity vector plots and velocity magnitude contour maps for inspiratory flow are shown in figure 6.10 for four nasal cross sections.

Pressure distributions along the lateral walls of the nasal cavity and iso-pressure surfaces are presented in figure 6.11, figure 6.12, figure 6.13 and figure 6.14 for inspiratory and expiratory cycles respectively. These figures represents that the simulation is able to give the correct distribution of the pressure inside nasal cavity.

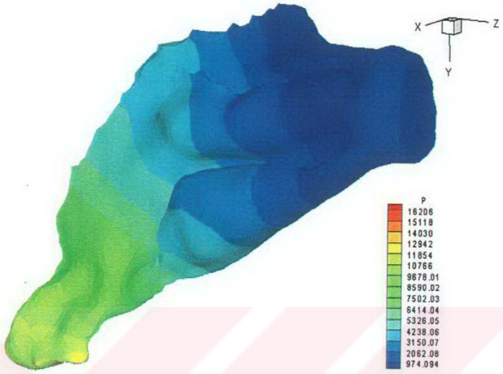

Figure 6.11 Pressure contours on lateral wall of the nasal cavity for inspiratory flow

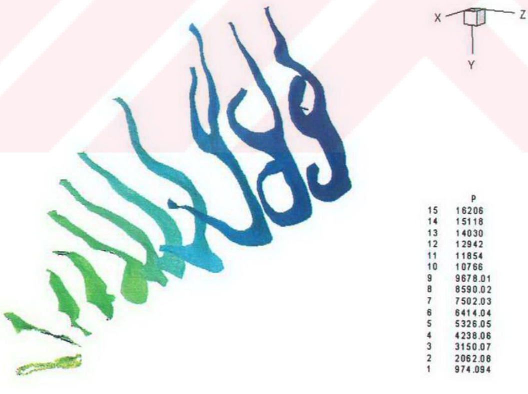

Figure 6.12 Pressure iso surfaces of the nasal cavity for inspiratory flow

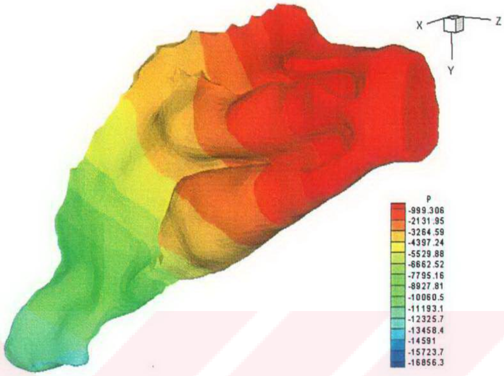

Figure 6.13 Pressure contours on lateral wall of the nasal cavity for expiratory flow

Figure 6.14 Pressure iso surfaces of the nasal cavity for expiratory flow

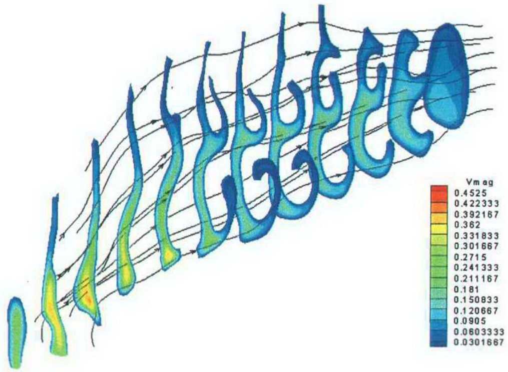

Figure 6.15 Stream traces with contours of velocity magnitude for inspiratory flow

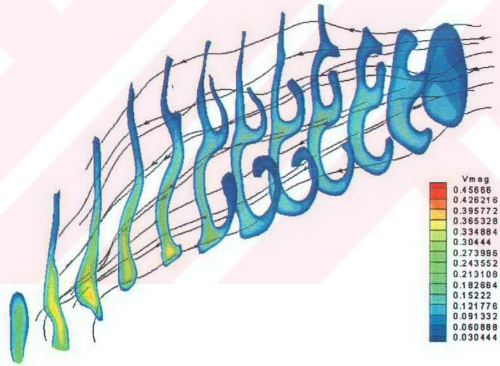

Figure 6.16 Stream traces with contours of velocity magnitude for expiratory flow

The flow inside the nasal cavity is also visualized using stream traces. The magnitude of the velocity of the flow is represented with different colors in figure 6.15 and 6.16 for inspiratory and expiratory cycles respectively. According to the results, inspiratory and expiratory airflow velocities are higher in the medial part of the nasal cavity.

7. CONCLUSIONS

The objective of this study is to analyze the fluid mechanic problems with finite element method. A hybrid grid for efficient representation of the boundary layer is implemented for the solution of steady laminar incompressible viscous flows.

An explicit finite element solver was used for the simulations. A commercial automatic mesh generation software was used to model the three dimensional geometries.

A pseudo-second order velocity/first order pressure elements are used. Hybrid tetrahedral grids consist of prismatic layers close to the body surface and tetrahedral elements inside the body are used to discretize the solution domain. The division of prismatic elements is explained in detail. Using prismatic elements close to the boundary provide correct representation of the boundary layer and the viscous region.

The three dimensional lid driven cavity flow is analyzed as a test case. The results show excellent agreement with the reference study.

The human nasal airflow is also simulated. The purposes of this numerical simulation were to determine the airflow profile in human nasal passages at steady state inspiration and expiration cycles, and to determine whether this CFD simulations of the airflow agreed with experiments.

Simulated velocity fields and pressure drops across the nasal cavity generally agreed with experimental results from the literature. The highest airspeeds are equally likely to occur in the middle of the nasal cavity which is in good agreement with those calculated by Keyhani et al [14].

REFERENCES

[1] **İDELSOHN, S. R., AND ONATE, E., (1994)**, 'Finite Volumes and Finite Elements: Two 'good friends'. Int. J. Numer. Methods Eng 37, 3323-3341.

[2] **LOHNER, R., (1987)**, 'Finite Elements in CFD: what lies ahead'. Int. J. Numer. Methods Eng 24, 1741-1756

[3] **NAKAJİMA, K., and KALLİNDERİS, Y., (1993)**, 'Comparison of finite element and finite volume methods for incompressible viscous flows', AIAA Journal 32, 5, 1090-1093.

[4] **TEZDUYAR, T. E., (2001)**, 'Finite Element Methods for Flow Problems with Moving Boundaries and Interfaces', Archives of Computational Methods in Engineering, 8, 83-130.

[5] **KWAK, D., (1989)**, 'Computation of Viscous Incompressible Flows', No. 1989-04 Von Karman Institute for Fluid Dynamics Lecture Series.

[6] **BROOKS, A., and HUGHES, T., (1982)**, 'Streamline upwind / Petrov Galerkin formulations for convective dominated flows with particular emphasis of the incompressible Navier-Stokes equations', Computer Methods in Applied Mechanics and Engineering, 32, 199-259.

[7] **EDIS, F. O., (1998)**, 'Efficient Finite Element Computation of Unsteady Incompressible Viscous Flows Using Pseudo-Second-Order Velocity Interpolation', Ph.D. Thesis, Istanbul Technical University.

[8] **SHERWİN, S. J., and PEİRO, J., (2002)**, 'Mesh Generation in Curvilinear Domains Using Higher-Order Elements', Int. J. Numer. Meth. Engng, 53, 207-223.

[9] **KALLİNDERİS, Y., and WARD, S., (1993)**, 'Prismatic Grid Generation for Three Dimensional Complex Geometries', AIAA Journal, 31:10, 1850-1856

[10] KALLİNDERİS, Y., and NAKAJIMA, K., (1994), 'Finite Element Method for Incompressible Viscous Flows with Adaptive Hybrid Grids', AIAA Journal, 32:8, 1617-1625

[11] KALLİNDERİS, Y., (1995), 'Adaptive Hybrid Prismatic/Tetrahedral Grids', Int. J. Numer. Meth. Engng, 20, 1023-1037

[12] KU, H., HİRSH, T., and TAYLOR, T., (1987), 'A pseudospectral method for solution of the three-dimensional incompressible Navier-Stokes equations', J. Comput. Phys. 59, 439-462.

[13] HAHN, İ., SCHERER, P. W., and MOZEL, M. M., (1993), 'Velocity profiles measured for airflow through a large-scale model of the human nasal cavity', J. Appl. Physiol. 75, 2273-2287

[14] KEYHANİ, K. and SCHERER, P. W., and MOZELL, M. M., (1995), 'Numerical Simulation of airflow in the human nasal cavity', J. Biomech. Eng. 117, 429-441.

[15] HORSCHLER, I., MEINKE, M., and SCHRODER, W., (2003), 'Numerical Simulation of the flow field in a model of the nasal cavity', Computers & Fluids 32, 39-45

[16] MYGIND, N, and DAHL, R., (1998), 'Anatomy, physiology and function of the nasal cavities in health and disease', Advanced Drug Delivery Reviews 29, 3-12

[17] SCHLICHTING, H., (1987), 'Boundary Layer Theory', McGraw-Hill, Inc, Seventh Edition

[18] MIZUKAMI, A., and TSUCHIYA M., (1984), 'A Finite Element Method for Three Dimensional non-steady Navier-Stokes Equations', Int. J. Numer. Methods Fluids 4.

[19] ROACHE, P., (1972), 'Computational Fluid Dynamics', First ed. Hermosa publishers, Albuquerque, NM.

[20] KALLİNDERİS, Y., (1992), 'Algebraic Turbulence Modelling for Adaptive Unstructured Grids', AIAA, 30, 631-639.

APPENDIX A.

The simulation results for the lid-driven cavity flow is represented in this section in detail.

a)

b)

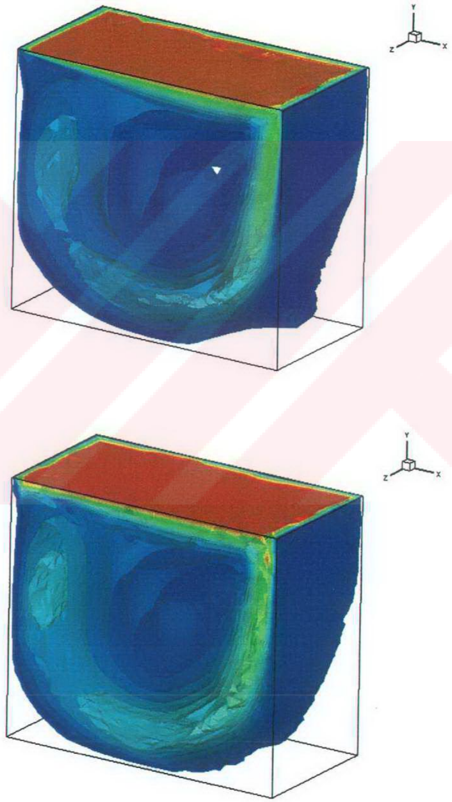

Figure A.1 Velocity magnitude iso-surface plots of lid-driven cavity flow a) tetra grid b) hybrid grid

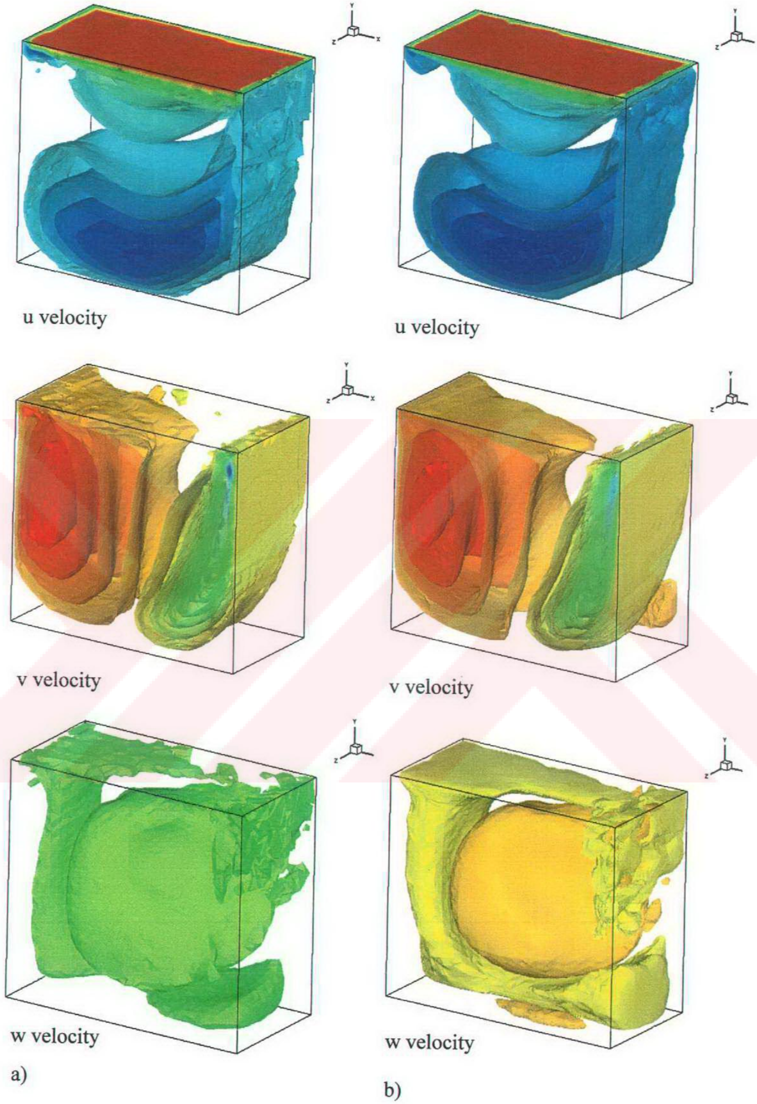

Figure A.2 Velocity components iso-surface plots of lid-driven cavity flow a) tetra grid b) hybrid grid

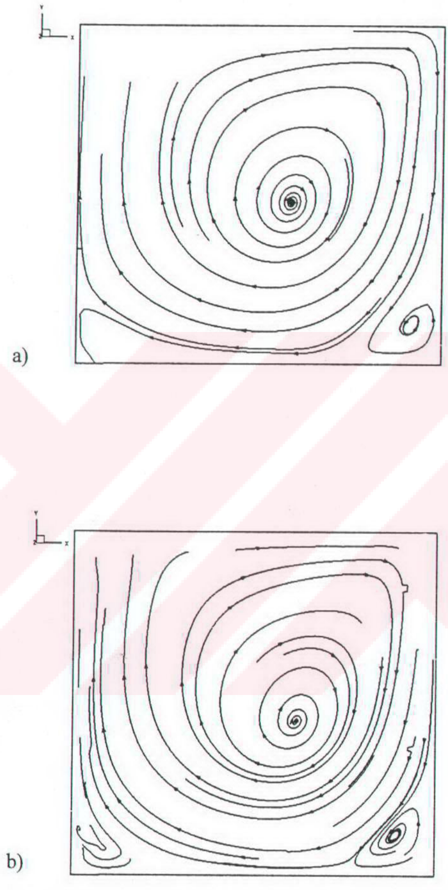

Figure A.3 Stream traces at the symmetry plane of lid driven cavity flow with a) tetra grid b) hybrid grid

VITA

She was born on April 12th, 1977 in Giresun. In 1994, she graduated from Giresun Anatolia High School. In 1995 she attended the Aerospace Engineering department in Istanbul Technical University. In 1997 she started her second major in Mechanical Engineerin in I.T.U. In 2000 she graduated as an honor student from Aerospace Engineering. Same year she attended the I.T.U. Institute of Science and Technology-Department of Aerospace Engineering. In 2001 she obtained her second BSc degree in Mechanical Engineering. She has been working as a research assistant in I.T.U. Faculty of Aeronautics and Astronautics since 2001. And she has been in Georgia Institute of Technology Department of Aerospace Engineering since January 2003 as a master student and graduate research assistant.